

Quantum Spin Dynamics in Molecular Magnets

Michael N. Leuenberger, Florian Meier, and Daniel Loss

*Department of Physics and Astronomy, University of Basel, Klingelbergstrasse 82, 4056 Basel,
Switzerland*

(October 22, 2018)

Summary. The detailed theoretical understanding of quantum spin dynamics in various molecular magnets is an important step on the roadway to technological applications of these systems. Quantum effects in both ferromagnetic and antiferromagnetic molecular clusters are, by now, theoretically well understood. Ferromagnetic molecular clusters allow one to study the interplay of incoherent quantum tunneling and thermally activated transitions between states with different spin orientation. The Berry phase oscillations found in Fe_8 are signatures of the quantum mechanical interference of different tunneling paths. Antiferromagnetic molecular clusters are promising candidates for the observation of coherent quantum tunneling on the mesoscopic scale. Although challenging, applications of molecular magnetic clusters for data storage and quantum data processing are within experimental reach already with present day technology.

Introduction

Molecular magnets have attracted considerable interest recently because of their potential for data storage and data processing [1]. In addition to possible future technological applications, molecular magnets are also interesting from an academic point of view because they show quantum effects on the mesoscopic scale [2] in the form of tunneling of magnetization. In the following, we review some of our theoretical work on quantum spin dynamics in molecular magnets.

Ferromagnetic molecular magnets such as Mn_{12} and Fe_8 show incoherent tunneling of the magnetization [3–6] and allow one to study the interplay of thermally activated processes and quantum tunneling. The spin tunneling leads to two effects. Firstly, the magnetization

relaxation is accelerated whenever spin states of opposite direction become degenerate due to the variation of the external longitudinal magnetic field [7–11]. Secondly, the spin acquires a Berry phase during the tunneling process, which leads to oscillations of the tunnel splitting as a function of the external transverse magnetic field [12–15].

Due to the strong quantum spin dynamics induced by antiferromagnetic exchange interaction [16–19], antiferromagnetic molecular magnets such as ferric wheels belong to the most promising candidates for the observation of coherent quantum tunneling on the mesoscopic scale [20–23]. In contrast to incoherent tunneling, in quantum coherent tunneling spins tunnel back and forth between energetically degenerate configurations at a tunneling rate which is *large* compared to the decoherence rate. The detection of coherent quantum tunneling is more challenging in antiferromagnetic molecular magnets than in ferromagnetic systems, but is feasible with present day experimental techniques.

Understanding the properties of molecular magnets is only a first step on the roadway to technological applications. A possible next step will be the preparation and control of a well defined single-spin quantum state of a molecular cluster. Although challenging, this task appears feasible with present day experiments and would allow one to carry out quantum computing with molecular magnets [1]. The idea is to use the Grover quantum search algorithm [24] to read-in and decode information stored in the phases of a single-spin state.

Spin tunneling in Mn_{12} -acetate

The magnetization relaxation of crystals and powders made of molecular magnets Mn_{12} has attracted much recent interest since several experiments [25–29] have indicated unusually long relaxation times as well as increased relaxation rates [7,8,30] whenever two spin states become degenerate in response to a varying longitudinal magnetic field H_z . According to earlier suggestions [31,27] this phenomenon has been interpreted as a manifestation of incoherent macroscopic quantum tunneling (MQT) of the spin.

As long as the external magnetic field H_z is much smaller than the internal exchange interactions between the Mn ions of the Mn_{12} cluster, the Mn_{12} cluster behaves like a large

single spin \mathbf{S} of length $s = 10$. For temperatures $T \gtrsim 1$ K its spin dynamics can be described by a spin Hamiltonian of form $\mathcal{H} = \mathcal{H}_a + \mathcal{H}_Z + \mathcal{H}_{\text{sp}} + \mathcal{H}_T$ including the coupling between this large spin and the phonons in the crystal [9–11,32–37]. In particular,

$$\mathcal{H}_a = -AS_z^2 - BS_z^4 \quad (1)$$

represents the magnetic anisotropy where $A \gg B > 0$. The Zeeman term through which the external magnetic field H_z couples to the spin \mathbf{S} is given by $\mathcal{H}_Z = g\mu_B H_z S_z$, while the tunneling between S_z -states is governed by

$$\mathcal{H}_T = -\frac{1}{2}B_4(S_+^4 + S_-^4) + g\mu_B H_x S_x, \quad (2)$$

where $H_x = |\mathbf{H}| \sin \theta$ ($\ll H_z$) is the transverse field, with θ being the misalignment angle. The values of the anisotropy constants A, B, B_4 have been determined by ESR experiments [38,39]. Finally, the most general spin-phonon coupling reads

$$\begin{aligned} \mathcal{H}_{\text{sp}} = & g_1(\epsilon_{xx} - \epsilon_{yy}) \otimes (S_x^2 - S_y^2) + \frac{1}{2}g_2\epsilon_{xy} \otimes \{S_x, S_y\} \\ & + \frac{1}{2}g_3(\epsilon_{xz} \otimes \{S_x, S_z\} + \epsilon_{yz} \otimes \{S_y, S_z\}) + \frac{1}{2}g_4(\omega_{xz} \otimes \{S_x, S_z\} + \omega_{yz} \otimes \{S_y, S_z\}), \end{aligned} \quad (3)$$

where g_i are the spin-phonon coupling constants, and $\epsilon_{\alpha\beta}$ ($\omega_{\alpha\beta}$) is the (anti-)symmetric part of the strain tensor. From the comparison between experimental data [7,8] and calculation it turns out that the constants $g_i \approx A \forall i$ [9–11].

We denote by $|m\rangle$, $-s \leq m \leq s$, the eigenstate of the unperturbed Hamiltonian $\mathcal{H}_a + \mathcal{H}_Z$ with eigenvalue $\varepsilon_m = -Am^2 - Bm^4 + g\mu_B H_z m$. If the external magnetic field H_z is increased one gets doubly degenerate spin states whenever a level m coincides with a level m' on the opposite side of the potential barrier. The resonance condition for double degeneracy, *i.e.* $\varepsilon_m = \varepsilon_{m'}$, leads to the resonance field

$$H_z^{mm'} = \frac{n}{g\mu_B} [A + B(m^2 + m'^2)]. \quad (4)$$

As usual, we refer to $n = m + m' = \text{even}$ (odd) as even (odd) resonances.

The relaxation of the magnetization is described in terms of a generalized master equation for the reduced density matrix $\rho(t)$ which includes off-diagonal terms due to resonances [9,10].

We use the notation $\rho_{mm'} = \langle m | \rho | m' \rangle$, $\rho_m = \langle m | \rho | m \rangle$. In the stationary limit $\dot{\rho}_{mm'} \approx 0$ a complete master equation

$$\dot{\rho}_m = -W_m \rho_m + \sum_{n \neq m, m'} W_{mn} \rho_n + \Gamma_m^{m'} (\rho_{m'} - \rho_m) \quad (5)$$

can be derived, where

$$\Gamma_m^{m'} = E_{mm'}^2 \frac{W_m + W_{m'}}{4\xi_{mm'}^2 + \hbar^2 (W_m + W_{m'})^2} \quad (6)$$

is the incoherent tunneling rate from m to m' in the presence of phonon-damping [10]. The spin-phonon rates $W_{m\pm 1, m}$ and $W_{m\pm 2, m}$ are evaluated by means of Fermi's golden rule [10].

In Refs. [9,10] the master equation is solved exactly to find the largest relaxation time. The result is plotted in Fig. 1. The even resonances are induced by the quartic B_4 -anisotropy, whereas the odd resonances are induced by product-combinations of $B_4 S_{\pm}^4$ - and $H_x S_x$ -terms. In Fig. 2 the peaks of the resonance at $H_z = 0$ (induced only by the B_4 -term) are displayed for four different temperatures. All the peaks are of single Lorentzian shape as a result of the 2-state transition rate $\Gamma_m^{m'}$ given in (6), which agrees well with the measurements [7].

It is instructive to determine the dominant transition paths via which the spin can relax. For this an approximate analytic expression for the relaxation time can be derived by means of conservation laws that resemble Kirchhoff's rules for electrical circuits [9,10].

Incoherent Zener tunneling in Fe_8

Besides Mn_{12} there have been several experiments on the molecular magnet Fe_8 that revealed macroscopic quantum tunneling of the spin [40–42,12,13]. In particular, recent measurements on Fe_8 [12,13] lead to the development of the concept of the incoherent Zener tunneling [14]. The resulting Zener tunneling probability P_{inc} exhibits Berry phase oscillations as a function of the external transverse field H_x .

For many physical systems the Landau-Zener model [43] has become an important tool for studying tunneling transitions [44–47]. It must be noted that all quantum systems to which the Zener model [43] is applicable can be described by *pure* states and their *coherent*

time evolution. Ref. [14] generalizes the Zener theory in the sense that also the *incoherent* evolution of *mixed* states is taken into account (see also Refs. [44] and [48–52] for a comparison). In particular, the theory presented in Ref. [14] agrees well with recent measurements of $P_{\text{inc}}(H_x)$ for various temperatures in Fe₈ [12,13].

For the Zener transition usually only the asymptotic limit is of interest. Therefore it is required that the range over which $\varepsilon_{mm'}(t) = \varepsilon_m - \varepsilon_{m'}$ is swept is much larger than the tunnel splitting $E_{mm'}$ and the decoherence rate $\hbar\gamma_{mm'}$ (see below and Fig. 3). In addition, the evolution of the spin system is restricted to times t that are much longer than the decoherence time $\tau_d = 1/\gamma_{mm'}$. In this case, tunneling transitions between pairs of degenerate excited states are incoherent. This tunneling is only observable if the temperature T is kept well below the activation energy of the potential barrier. Accordingly, one is interested only in times t that are larger than the relaxation times of the excited states. Thus, the formalism presented in Refs. [9,10] can be applied. It was shown in Ref. [14] that the Zener tunneling can be described by Eq. (5), where

$$\Gamma_m^{m'}(t) = \frac{E_{mm'}^2}{2} \frac{\gamma_{mm'}}{\varepsilon_{mm'}^2(t) + \hbar^2 \gamma_{mm'}^2} \quad (7)$$

is time-dependent, in contrast to Eq. (6). As usual, the abbreviations $\gamma_{mm'} = (W_m + W_{m'})/2$ and $W_m = \sum_n W_{nm}$ are used, where W_{nm} denotes the approximately time-independent transition rate from $|m\rangle$ to $|n\rangle$, which can be obtained via Fermi's golden rule [9,10]. The tunnel splitting [9,10] is given by

$$E_{mm'} = 2 \left| \sum_{\substack{m_1, \dots, m_N \\ m_i \neq m, m'}} \frac{V_{m, m_1}}{\varepsilon_m - \varepsilon_{m_1}} \prod_{i=1}^{N-1} \frac{V_{m_i, m_{i+1}}}{\varepsilon_m - \varepsilon_{m_{i+1}}} V_{m_N, m'} \right|. \quad (8)$$

V_{m_i, m_j} denote off-diagonal matrix elements of the total Hamiltonian \mathcal{H}_{tot} .

Since all resonances n lead to similar results, Eq. (5) is solved only in the unbiased case — corresponding to $n = 0$ (see below) — where the ground states $|s\rangle$, $|-s\rangle$ and the excited states $|m\rangle$, $| -m\rangle$, $m \in [[s] - s + 1, s - 1]$ of the spin system with spin s are pairwise degenerate. In addition, it is assumed that the excited states are already in their stationary state, i.e., $\dot{\rho}_m = 0 \ \forall m \neq s, -s$. Eq. (5) leads then to

$$1 - P_{\text{inc}} \equiv \Delta\rho(t) = \exp \left\{ - \int_{t_0}^t dt' \Gamma_{\text{tot}}(t') \right\}, \quad (9)$$

where $\Delta\rho(t) = \rho_s - \rho_{-s}$, which satisfies the initial condition $\Delta\rho(t = t_0) = 1$, and thus $P_{\text{inc}}(t = t_0) = 0$. The total time-dependent relaxation rate is given by $\Gamma_{\text{tot}} = 2[\Gamma_s^{-s} + \Gamma_{\text{th}}]$, where the thermal rate Γ_{th} , which determines the incoherent relaxation via the excited states, is evaluated by means of relaxation diagrams [9,10].

Assuming linear time dependence, i.e., $\varepsilon_{mm'}(t) = \alpha_m^{m'} t$, in the transition region [43], and with $|\varepsilon_{mm'}^{\langle, \rangle}| \gg \hbar\gamma_{mm'}$ one obtains from Eq. (9)

$$\begin{aligned} \Delta\rho &= \exp \left\{ - \frac{2E_{s,-s}^2}{\hbar\alpha_s^{-s}} \arctan \left(\frac{\alpha_s^{-s}}{\hbar\gamma_{s,-s}} t \right) - \int_{-t}^t dt' \Gamma_{\text{th}} \right\} \\ &\approx \exp \left\{ - \frac{\pi E_{s,-s}^2}{\hbar\alpha_s^{-s}} - \int_{-t}^t dt' \Gamma_{\text{th}} \right\}, \end{aligned} \quad (10)$$

where $t_0 = -t$. In the low-temperature limit $T \rightarrow 0$ the excited states are not populated anymore and thus Γ_{th} , which consists of intermediate rates that are weighted by Boltzmann factors b_m [9,10], vanishes. Consequently, Eq. (10) simplifies to

$$\Delta\rho = \exp \left\{ - \frac{\pi E_{s,-s}^2}{\hbar\alpha_s^{-s}} \right\} = \exp \left\{ - \frac{\pi E_{s,-s}^2}{\hbar |\dot{\varepsilon}_{s,-s}(0)|} \right\}. \quad (11)$$

The exponent in Eq. (11) differs by a factor of 2 from the Zener exponent [43]. This is not surprising since Γ_{tot} is the relaxation rate of $\Delta\rho$, where both ρ_s and ρ_{-s} are changed in time by the same amount, and *not* an escape rate like in the case of coherent Zener transition, where only the population of the initial state is changed in time. Eq. (11) implies $P_{\text{inc}} = 1$ for $|\dot{\varepsilon}_{s,-s}(0)| \rightarrow 0$ (adiabatic limit) and $P_{\text{inc}} = 0$ for $|\dot{\varepsilon}_{s,-s}(0)| \rightarrow \infty$ (sudden limit).

In accordance with earlier work [12,13,40–42,53] Ref. [14] uses a single-spin Hamiltonian $\mathcal{H} = \mathcal{H}_a + \mathcal{H}_T + \mathcal{H}_Z + \mathcal{H}_{\text{sp}}$ that describes sufficiently well the behavior of the large spin \mathbf{S} with $s = 10$ of a Fe_8 cluster. After fitting the parameters the incoherent Zener theory is in excellent agreement with experiments [12,13] for the temperature range $0.05 \text{ K} \leq T \leq 0.7 \text{ K}$ if the states $|\pm 10\rangle$, $|\pm 9\rangle$, and $|\pm 8\rangle$ are taken into account. In particular, the path leading through $|\pm 8\rangle$ gives a non-negligible contribution for $T \gtrsim 0.6 \text{ K}$. Solving the relaxation diagram shown in Fig. 4 one obtains from Eq. (10) for Fe_8 in the case $n = 0$

$$\Gamma_{\text{tot}} = 2 \left(\Gamma_{10}^{-10} + \sum_{n=9}^8 \frac{b_n}{\frac{2}{W_{10,n}} + \frac{1}{\Gamma_n^{-n}}} \right), \quad (12)$$

$$\Delta\rho = \exp \left\{ -\frac{\pi E_{10,-10}^2}{\hbar \alpha_{10}^{-10}} - \sum_{n=9}^8 \frac{\pi E_{n,-n}^2 W_{10,n} b_n}{\alpha_n^{-n} \sqrt{E_{n,-n}^2 + \hbar^2 W_{10,n}^2}} \right\},$$

where the approximation $\gamma_{n,-n} \approx W_{10,n}$ and $|\varepsilon_{mm'}^{<,>}| \gg E_{n,-n}, \gamma_{n,-n}$ is used. $P_{\text{inc}} = 1 - \Delta\rho$, which is plotted in Fig. 5, is in good agreement with the measurements [13].

Coherent Néel vector tunneling in antiferromagnetic molecular wheels

Antiferromagnetic molecular clusters belong to the most promising candidates for the observation of coherent quantum tunneling on the mesoscopic scale currently available [20]. Several systems in which an even number N of antiferromagnetically coupled ions is arranged on a ring have been synthesized to date [54–57]. These systems are well described by the spin Hamiltonian

$$\hat{H} = J \sum_{i=1}^N \hat{\mathbf{s}}_i \cdot \hat{\mathbf{s}}_{i+1} + g\mu_B \mathbf{B} \cdot \sum_{i=1}^N \hat{\mathbf{s}}_i - k_z \sum_{i=1}^N \hat{s}_{i,z}^2, \quad (13)$$

where $\hat{\mathbf{s}}_i$ is the spin operator at site i with spin quantum number s , $\hat{\mathbf{s}}_{N+1} \equiv \hat{\mathbf{s}}_1$, J is the nearest-neighbor exchange, \mathbf{B} the magnetic field, and $k_z > 0$ the single-ion anisotropy directed along the ring axis. The parameters J and k_z have been well established both for various ferric wheels [54–56, 58–62] with $N = 6, 8, 10$, and, more recently, also for a Cr wheel [57]. For $\mathbf{B} = 0$, the classical ground-state spin configuration of the wheel shows alternating (Néel) order with the spins pointing along $\pm \mathbf{e}_z$. The two states with the Néel vector \mathbf{n} along $\pm \mathbf{e}_z$ [Fig. 6], labeled $|\uparrow\rangle$ and $|\downarrow\rangle$, are energetically degenerate and separated by an energy barrier of height $Nk_z s^2$. Because antiferromagnetic exchange induces dynamics of Néel ordered spins, the states $|\uparrow\rangle$ and $|\downarrow\rangle$ are not energy eigenstates. Rather, a molecule prepared in spin state $|\uparrow\rangle$ would tunnel coherently between $|\uparrow\rangle$ and $|\downarrow\rangle$ at a rate Δ/\hbar , where Δ is the tunnel splitting [16,17]. This tunneling of the Néel vector corresponds to a simultaneous tunneling of all N spins within the wheel through a potential barrier governed by the easy-axis anisotropy. Within the framework of coherent state spin path integrals,

an explicit expression for the tunnel splitting Δ as a function of the magnetic field \mathbf{B} has been derived [20]. A magnetic field applied in the ring plane, B_x , gives rise to a Berry phase acquired by the spins during tunneling [15,63]. The resulting interference of different tunneling paths leads to a sinusoidal dependence of Δ on B_x , which allows one to continuously tune the tunnel splitting from 0 to a maximum value which is of order of some Kelvin for the antiferromagnetic wheels synthesized to date.

The tunnel splitting Δ also enters the energy spectrum of the antiferromagnetic wheel as level spacing between the ground and first excited state. Thus, Δ can be experimentally determined from various quantities such as magnetization, static susceptibility, and specific heat. Even more information on the physical properties of antiferromagnetic wheels [Eq. (13)] can be obtained from a theoretical and experimental investigation of dynamical quantities, such as the correlation functions of the total spin $\hat{\mathbf{S}} = \sum_{i=1}^N \hat{\mathbf{s}}_i$ or of single spins within the wheel [21–23]. By symmetry arguments, it follows that the correlation function of total spin, $\langle \hat{S}_\alpha(t) \hat{S}_\alpha(0) \rangle$, which is experimentally accessible via measurement of the alternating current (AC) susceptibility does not contain a component which oscillates with the tunnel frequency Δ/h [21–23]. Hence, neither the tunnel splitting nor the decoherence rate of Néel vector tunneling can be obtained by experimental techniques which couple to the *total* spin of the wheel. In contrast, the correlation function of a single spin

$$\langle \hat{s}_{i,z}(t) \hat{s}_{i,z}(0) \rangle \simeq s^2 \left(\frac{e^{-\beta\Delta/2}}{2 \cosh(\beta\Delta/2)} e^{i\Delta t/\hbar} + \frac{e^{\beta\Delta/2}}{2 \cosh(\beta\Delta/2)} e^{-i\Delta t/\hbar} \right) \quad (14)$$

exhibits the time dependence characteristic of coherent tunneling of the quantity $\hat{s}_{i,z}$ with a tunneling rate Δ/h [21]. We conclude that *local* spin probes are required for the observation of the Néel vector dynamics. Nuclear spins which couple (predominantly) to a given single spin $\hat{\mathbf{s}}_i$ are ideal candidates for such probes [21] and have already been used to study spin cross-relaxation between electron and nuclear spins in ferric wheels [64,65].

For simplicity, we consider a single nuclear spin $\hat{\mathbf{I}}$, $I = 1/2$, coupled to one electron spin by a hyperfine contact interaction $\hat{H}' = A \hat{\mathbf{s}}_1 \cdot \hat{\mathbf{I}}$. According to Eq. (14), the tunneling electron spin $\hat{\mathbf{s}}_1$ produces a rapidly oscillating hyperfine field $As \cos(\Delta t/\hbar)$ at the site of the

nucleus. Signatures of the coherent electron spin tunneling can thus also be found in the nuclear susceptibility. For a static magnetic field applied in the plane of the ring, B_x , it can be shown that the nuclear susceptibility

$$\begin{aligned} \chi''_{I,yy}(\omega) &\simeq \frac{\pi}{4} \left[\tanh\left(\frac{\beta\gamma_I B_x}{2}\right) \delta(\omega - \gamma_I B_x/\hbar) \right. \\ &\quad \left. + \left(\frac{As}{\Delta}\right)^2 \tanh\left(\frac{\beta\Delta}{2}\right) \delta(\omega - \Delta/\hbar) \right] - [\omega \rightarrow -\omega] \end{aligned} \quad (15)$$

exhibits a *satellite resonance at the tunnel splitting Δ of the electron spin system* [21]. Here, $\gamma_I B_x$ is the Larmor frequency of the nuclear spin and the first term in Eq. (15) corresponds to the transition between the Zeeman-split energy levels of I . Because typically $As \simeq 1$ mK and $\Delta \lesssim 2$ K in Fe₁₀, the spectral weight of the satellite peak is small compared to the one of the first term in Eq. (15) unless the magnetic field is tuned such that Δ is significantly reduced compared to its maximum value. The observation of the satellite peak in $\chi''_{I,yy}(\omega)$ is challenging, but possible with current experimental techniques [21]. The experiment must be conducted with single crystals of an antiferromagnetic molecular wheel with sufficiently large anisotropy $k_z > 2J/(Ns)^2$ at high, tunable fields (10 T) and low temperatures (2 K). Moreover, because the tunnel splitting $\Delta(\mathbf{B})$ depends sensitively on the relative orientation of \mathbf{B} and the easy axis [59,60], careful field sweeps are necessary to ensure that the satellite peak in Eq. (15) has a large spectral weight.

The need for local spin probes such as NMR or inelastic neutron scattering to detect coherent Néel vector tunneling can be traced back to the translation symmetry of the spin Hamiltonian \hat{H} [22,23]. If this symmetry is broken, e.g. by doping of the wheel, ESR also provides an adequate technique for the detection of coherent Néel vector tunneling. If one of the original Fe or Cr ions of the wheel with spin $s = 5/2$ or $s = 3/2$, respectively, is replaced by an ion with different spin $s' \neq s$, this will in general also result in a different exchange constant J' and single ion anisotropy k'_z at the dopand site, i.e.,

$$\hat{H} = J \sum_{i=2}^{N-1} \hat{\mathbf{s}}_i \cdot \hat{\mathbf{s}}_{i+1} + J'(\hat{\mathbf{s}}_1 \cdot \hat{\mathbf{s}}_2 + \hat{\mathbf{s}}_1 \cdot \hat{\mathbf{s}}_N) + g\mu_B \mathbf{B} \cdot \sum_{i=1}^N \hat{\mathbf{s}}_i - (k'_z \hat{s}_{1,z}^2 + k_z \sum_{i=2}^N \hat{s}_{i,z}^2). \quad (16)$$

Although thermodynamic quantities, such as magnetization, of the doped wheel may differ significantly from the ones of the undoped wheel, the picture of spin tunneling in antiferromagnetic molecular systems [16,17] remains valid [22]. However, due to unequal sublattice spins, a net total spin remains even in the Néel ordered state of the doped wheel [Fig. 7] which allows one to distinguish the configurations sketched in Fig. 6 according to their total spin. The dynamics of the total spin $\hat{\mathbf{S}}$ is coupled to the one of the Néel vector, and coherent tunneling of the Néel vector results in a coherent oscillation of the total spin such that the tunneling dynamics can also be probed by ESR. The AC susceptibility shows a resonance peak at the tunnel splitting Δ ,

$$\chi''_{zz}(\omega \simeq \Delta/\hbar) = \pi(g\mu_B)^2 |\langle e|\hat{S}_z|g\rangle|^2 \tanh\left(\frac{\beta\Delta}{2}\right) \delta(\omega - \Delta/\hbar). \quad (17)$$

with a transition matrix element between the ground state $|g\rangle$ and first excited state $|e\rangle$,

$$|\langle e|\hat{S}_z|g\rangle| \simeq |s' - s| \frac{8Jk_z s^2}{(g\mu_B B_x)^2} \quad (18)$$

for $g\mu_B B_x \gg s\sqrt{8Jk_z}$. The matrix element in Eq. (18) determines the spectral weight of the absorption peak in the ESR spectrum. The analytical dependence has been determined within a semiclassical framework and is in good agreement with numerical results obtained from exact diagonalization of small systems [Fig. 7].

In conclusion, several antiferromagnetic molecular wheels synthesized recently are promising candidates for the observation of coherent Néel vector tunneling. Although the observation of this phenomenon is experimentally challenging, nuclear magnetic resonance, inelastic neutron scattering, and ESR on doped wheels are adequate experimental techniques. The theory of coherent spin quantum tunneling as presented above applies to zero-dimensional systems, such as small ferric wheels. With increasing wheel size, the possibility of different magnetic domains arises and new exciting quantum effects in the dynamics of domain walls come into play [66–72]. Molecular wheels will also allow one to study the transition from zero- to one-dimensional quantum behavior with increasing system size.

Quantum computing with molecular magnets

Shor and Grover demonstrated that a quantum computer can outperform any classical computer in factoring numbers [73] and in searching a database [24] by exploiting the parallelism of quantum mechanics. Recently, the latter has been successfully implemented [74] using Rydberg atoms. In Ref. [1] an implementation of Grover's algorithm was proposed that uses molecular magnets [7,8,13,41,75]. It was shown theoretically that molecular magnets can be used to build dense and efficient memory devices based on the Grover algorithm. In particular, one single crystal can serve as a storage unit of a dynamic random access memory device. Fast electron spin resonance pulses can be used to decode and read out stored numbers of up to 10^5 , with access times as short as 10^{-10} seconds. This proposal should be feasible using the molecular magnets Fe_8 and Mn_{12} .

Suppose we want to find a phone number in a phone book consisting of $N = 2^n$ entries. Usually it takes $N/2$ queries on average to be successful. Even if the N entries were encoded binary, a classical computer would need approximately $\log_2 N$ queries to find the desired phone number [24]. But the computational parallelism provided by the superposition and interference of quantum states enables the Grover algorithm to reduce the search to one single query [24]. This query can be implemented in terms of a unitary transformation applied to the single spin of a molecular magnet. Such molecular magnets, forming identical and largely independent units, are embedded in a single crystal so that the ensemble nature of such a crystal provides a natural amplification of the magnetic moment of a single spin. However, for the Grover algorithm to succeed, it is necessary to find ways to generate arbitrary superpositions of spin eigenstates. For spins larger than $1/2$ this turns out to be a highly non-trivial task as spin excitations induced by magnetic dipole transitions in conventional electron spin resonance (ESR) can change the magnetic quantum number m by only ± 1 . To circumvent such physical limitations it was proposed to use multifrequency coherent magnetic radiation that allows the controlled generation of arbitrary spin superpositions. In particular, it was shown that by means of advanced ESR techniques it is possible to coherently populate and manipulate many spin states simultaneously by applying one single

pulse of a magnetic a.c. field containing an appropriate number of matched frequencies. This a.c. field creates a nonlinear response of the magnet via multiphoton absorption processes involving particular sequences of σ and π photons which allows the encoding and, similarly, the decoding of states. Finally, the subsequent read-out of the decoded quantum state can be achieved by means of pulsed ESR techniques. These exploit the non-equidistance of energy levels which is typical of molecular magnets.

Molecular magnets have the important advantage that they can be grown naturally as single crystals of up to 10-100 μm length containing about 10^{12} to 10^{15} (largely) independent units so that only minimal sample preparation is required. The molecular magnets are described by a single-spin Hamiltonian of the form $\mathcal{H}_{\text{spin}} = \mathcal{H}_a + V + \mathcal{H}_{\text{sp}} + \mathcal{H}_T$ [9,10,14], where $\mathcal{H}_a = -AS_z^2 - BS_z^4$ represents the magnetic anisotropy ($A \gg B > 0$). The Zeeman term $V = g\mu_B \mathbf{H} \cdot \mathbf{S}$ describes the coupling between the external magnetic field \mathbf{H} and the spin \mathbf{S} of length s . The calculational states are given by the $2s + 1$ eigenstates of $\mathcal{H}_a + g\mu_B H_z S_z$ with eigenenergies $\varepsilon_m = -Am^2 - Bm^4 + g\mu_B H_z m$, $-s \leq m \leq s$. The corresponding classical anisotropy potential energy $E(\theta) = -As \cos^2 \theta - Bs \cos^4 \theta + g\mu_B H_z s \cos \theta$, is obtained by the substitution $S_z = s \cos \theta$, where θ is the polar spherical angle. We have introduced the notation $m, m' = m - m'$. By applying a bias field H_z such that $g\mu_B H_z > E_{mm'}$, tunneling can be completely suppressed and thus \mathcal{H}_T can be neglected [9,10,14]. For temperatures of below 1 K transitions due to spin-phonon interactions (\mathcal{H}_{sp}) can also be neglected. In this regime, the level lifetime in Fe_8 and Mn_{12} is estimated to be about $\tau_d = 10^{-7}\text{s}$, limited mainly by hyperfine and/or dipolar interactions [1].

Since the Grover algorithm requires that all the transition probabilities are almost the same, Ref. [1] proposes that all the transition amplitudes between the states $|s\rangle$ and $|m\rangle$, $m = 1, 2, \dots, s-1$, are of the same order in perturbation V . This allows us to use perturbation theory. A different approach uses the magnetic field amplitudes to adjust the appropriate transition amplitudes [76]. Both methods work only if the energy levels are not equidistant, which is typically the case in molecular magnets owing to anisotropies. In general, if we choose to work with the states $m = m_0, m_0 + 1, \dots, s-1$, where $m_0 = 1, 2, \dots, s-1$, we have

to go up to n th order in perturbation, where $n = s - m_0$ is the number of computational states used for the Grover search algorithm (see below), to obtain the first non-vanishing contribution. Fig. 9 shows the transitions for $s = 10$ and $m_0 = 5$. The n th-order transitions correspond to the nonlinear response of the spin system to strong magnetic fields. Thus, a coherent magnetic pulse of duration T is needed with a discrete frequency spectrum $\{\omega_m\}$, say, for Mn_{12} between 20 and 300 GHz and a single low-frequency 0 around 100 MHz. The low-frequency field $\mathbf{H}_z(t) = H_0(t) \cos(\omega_0 t) \mathbf{e}_z$, applied along the easy-axis, couples to the spin of the molecular magnet through the Hamiltonian

$$V_{\text{low}} = g\mu_B H_0(t) \cos(\omega_0 t) S_z, \quad (19)$$

where $\hbar\omega_0 \ll \varepsilon_{m_0} - \varepsilon_{m_0+1}$ and \mathbf{e}_z is the unit vector pointing along the z axis. The π photons of V_{low} supply the necessary energy for the resonance condition (see below). They give rise to virtual transitions with $\Delta m = 0$, that is, they do not transfer any angular momentum, see Fig. 9. The perturbation Hamiltonian for the high-frequency transitions from $|s\rangle$ to virtual states that are just below $|m\rangle$, $m = m_0, \dots, s-1$, given by the transverse fields $\mathbf{H}_{\perp}^{-}(t) = \sum_{m=m_0}^{s-1} H_m(t) [\cos(\omega_m t + \Phi_m) \mathbf{e}_x - \sin(\omega_m t + \Phi_m) \mathbf{e}_y]$, reads

$$\begin{aligned} V_{\text{high}}(t) &= \sum_{m=m_0}^{s-1} g\mu_B H_m(t) [\cos(\omega_m t + \Phi_m) S_x - \sin(\omega_m t + \Phi_m) S_y] \\ &= \sum_{m=m_0}^{s-1} \frac{g\mu_B H_m(t)}{2} [e^{i(\omega_m t + \Phi_m)} S_+ + e^{-i(\omega_m t + \Phi_m)} S_-], \end{aligned} \quad (20)$$

with phases Φ_m (see below), where we have introduced the unit vectors \mathbf{e}_x and \mathbf{e}_y pointing along the x and y axis, respectively. These transverse fields rotate clockwise and thus produce left circularly polarized σ^- photons which induce only transitions in the left well (see Fig. 8). In general, absorption (emission) of σ^- photons gives rise to $\Delta m = -1$ ($\Delta m = +1$) transitions, and vice versa in the case of σ^+ photons. Anti-clockwise rotating magnetic fields of the form $\mathbf{H}_{\perp}^{+}(t) = \sum_{m=m_0}^{s-1} H_m(t) [\cos(\omega_m t + \Phi_m) \mathbf{e}_x + \sin(\omega_m t + \Phi_m) \mathbf{e}_y]$ can be used to induce spin transitions only in the right well (see Fig. 8)). In this way, both wells can be accessed independently.

Next we calculate the quantum amplitudes for the transitions induced by the magnetic a.c. fields (see Fig. 9) by evaluating the S -matrix perturbatively. The j th-order term of the perturbation series of the S -matrix in powers of the total perturbation Hamiltonian $V(t) = V_{\text{low}}(t) + V_{\text{high}}(t)$ is expressed by

$$S_{m,s}^{(j)} = \left(\frac{1}{i\hbar}\right)^j \prod_{k=1}^{j-1} \int_{-\infty}^{\infty} dt_k \int_{-\infty}^{\infty} dt_j \Theta(t_k - t_{k+1}) \times U(\infty, t_1) V(t_1) U(t_1, t_2) V(t_2) \dots V(t_j) U(t_j, -\infty), \quad (21)$$

which corresponds to the sum over all Feynman diagrams \mathcal{F} of order j , and where $U(t, t_0) = e^{-i(\mathcal{H}_a + g\mu_B \delta H_z)(t-t_0)/\hbar}$ is the free propagator, $\Theta(t)$ is the Heavyside function. The total S -matrix is then given by $S = \sum_{j=0}^{\infty} S^{(j)}$. The high-frequency virtual transition changing m from s to $s-1$ is induced by the frequency $\omega_{s-1} = \omega_{s-1,s} - (n-1)\omega_0$. The other high frequencies ω_m , $m = m_0, \dots, s-2$, of the high-frequency fields H_m mismatch the level separations by ω_0 , that is, $\hbar\omega_m = \varepsilon_m - \varepsilon_{m+1} + \hbar\omega_0$, see Fig. 9. As the levels are not equidistant, it is possible to choose the low and high frequencies in such a way that $S_{m,s}^{(j)} = 0$ for $j < n$, in which case the resonance condition is not satisfied, that is, energy is not conserved. In addition, the higher-order amplitudes $|S_{m,s}^{(j)}|$ are negligible compared to $|S_{m,s}^{(j)}|$ for $j > n$. Using rectangular pulse shapes, $H_k(t) = H_k$, if $-T/2 < t < T/2$, and 0 otherwise, for $k = 0$ and $k \geq m_0$, one obtains ($m \geq m_0$)

$$S_{m,s}^{(n)} = \sum_{\mathcal{F}} \Omega_m \frac{2\pi}{i} \left(\frac{g\mu_B}{2\hbar}\right)^n \frac{\prod_{k=m}^{s-1} H_k e^{-i\Phi_k} H_0^{m-m_0} p_{m,s}(\mathcal{F})}{(-1)^{q_{\mathcal{F}}} q_{\mathcal{F}}! r_s(\mathcal{F})! \omega_0^{n-1}} \times \delta^{(T)}(\omega_{m,s} - \sum_{k=m}^{s-1} \omega_k - (m-m_0)\omega_0), \quad (22)$$

where $\Omega_m = (m-m_0)!$, is the symmetry factor of the Feynman diagrams \mathcal{F} (see Fig. 9), $q_{\mathcal{F}} = m - m_0 - r_s(\mathcal{F})$, $p_{m,s}(\mathcal{F}) = \prod_{k=m}^s \langle k | S_z | k \rangle^{r_k(\mathcal{F})}$, $r_k(\mathcal{F}) = 0, 1, 2, \dots, \leq m - m_0$ is the number of π transitions directly above or below the state $|k\rangle$, depending on the particular Feynman diagram \mathcal{F} , and $\delta^{(T)}(\omega) = \frac{1}{2\pi} \int_{-T/2}^{+T/2} e^{i\omega t} dt = \sin(\omega T/2)/\pi\omega$ is the delta-function of width $1/T$, ensuring overall energy conservation for $\omega T \gg 1$. The duration T of the magnetic pulses must be shorter than the lifetimes τ_d of the states $|m\rangle$ (see Fig. 8).

In general the magnetic field amplitudes H_k must be chosen in such a way that perturbation theory is still valid and the transition probabilities are almost equal, which is required by the Grover algorithm. In Ref. [1] the amplitudes H_k do not differ too much from each other due to the partial destructive interference of the different transition diagrams shown in Fig. 8. Ref. [76] shows that the transition probabilities can be increased by increasing both the magnetic field amplitudes and the detuning energies under the condition that the magnetic field amplitudes remain smaller than the detuning energies. In this way, both high multiphoton Rabi oscillation frequencies and small quantum computation times can be attained. This makes both methods [1,76] very robust against decoherence sources.

In order to perform the Grover algorithm, one needs the relative phases φ_m between the transition amplitudes $S_{m,s}^{(n)}$, which is determined by $\Phi_m = \sum_{k=s-1}^{m+1} \Phi_k + \varphi_m$, where Φ_m are the relative phases between the magnetic fields $H_m(t)$. In this way, it is possible to read-in and decode the desired phases Φ_m for each state $|m\rangle$. The read-out is performed by standard spectroscopy with pulsed ESR, where the circularly polarized radiation can now be incoherent because only the absorption intensity of only one pulse is needed. Fig. 10 shows an example where the state $|7\rangle$ is populated within the computational basis (excluding the ground state). Then, we would observe only transitions from $|7\rangle$ to $|8\rangle$ at the frequency $\omega = \omega_{8,7}$ and transitions from $|7\rangle$ to $|6\rangle$ at $\omega = \omega_{6,7}$, which uniquely identifies the populated level, because the levels are not equidistant. This spectrum identifies all the populated states unambiguously. Alternatively, one could measure the magnetization of the sample with a high precision (see e.g. Ref. [77]). We emphasize that the entire Grover algorithm (read-in, decoding, read-out) requires three subsequent pulses each of duration T with $\tau_d > T > \omega_0^{-1} > \omega_m^{-1} > \omega_{m,m\pm 1}^{-1}$. This gives a 'clock-speed' of about 10 GHz for Mn_{12} , that is, the entire process of read-in, decoding, and read-out can be performed within about 10^{-10} s.

The proposal for implementing Grover's algorithm works not only for molecular magnets but for any electron or nuclear spin system with non-equidistant energy levels, as is shown in Ref. [76] for nuclear spins in GaAs semiconductors. Instead of storing information in the phases of the eigenstates $|m\rangle$ [1], in Ref. [76] the eigenenergies of $|m\rangle$ in the generalized

rotating frame are used for encoding information. The decoding is performed by bringing the delocalized state $(1/\sqrt{n}) \sum_m |m\rangle$ into resonance with $|m\rangle$ in the generalized rotating frame. Although such spin systems cannot be scaled to arbitrarily large spin s — the larger a spin becomes, the faster it decoheres and the more classical its behavior will be — we can use such spin systems of given s to great advantage in building dense and highly efficient memory devices.

For a first test of the nonlinear response, one can irradiate the molecular magnet with an a.c. field of frequency $\omega_{s-2,s}/2$, which gives rise to a two-photon absorption and thus to a Rabi oscillation between the states $|s\rangle$ and $|s-2\rangle$. For stronger magnetic fields it is in principle possible to generate superpositions of Rabi oscillations between the states $|s\rangle$ and $|s-1\rangle$, $|s\rangle$ and $|s-2\rangle$, $|s\rangle$ and $|s-3\rangle$, and so on (see also Ref. [76]).

Acknowledgements: This work has been supported by the EU network Molnanomag, the BBW Bern, the Swiss National Science Foundation, DARPA, and ARO.

REFERENCES

- [1] Leuenberger MN, Loss D (2001) *Nature* **410**: 789
- [2] Leggett AJ in *Quantum tunneling of Magnetization*, edited by Gunther L and Barbara B (Kluwer, Dodrecht, 1995), p.1
- [3] Korenblit IYa, Shender EF (1978) *Sov Phys JETP* **48**: 937
- [4] van Hemmen JL, Sütö A (1986) *Europhys Lett* **1**: 481; (1986) *Physica B* **141**: 37
- [5] Enz M, Schilling R (1986) *J Phys C: Solid State Phys* **19**: L711; (1986) *J Phys C: Solid State Phys* **19**: 1765
- [6] Chudnovsky EM, Gunther L (1988) *Phys Rev Lett* **60**: 661
- [7] Friedman JR, Sarachik MP, Tejada J, Ziolo R (1996) *Phys Rev Lett* **76**: 3830
- [8] Thomas L, Lioni F, Ballou R, Gatteschi D, Sessoli R, Barbara B (1996) *Nature (London)* **383**: 145
- [9] Leuenberger MN, Loss D (1999) *Europhys Lett* **46**: 692
- [10] Leuenberger MN, Loss D (2000) *Phys. Rev. B* **61**: 1286
- [11] Leuenberger MN, Loss D (2000) *Europhys. Lett.* **52**: 247
- [12] Wernsdorfer W, Sessoli R (1996) *Science* **284**: 133
- [13] Wernsdorfer W, Sessoli R, Caneschi A, Gatteschi D, Cornia A (2000) *Europhys Lett* **50**: 552
- [14] Leuenberger MN, Loss D (2000) *Phys Rev B* **61**: 12200
- [15] Loss D, DiVincenzo DP, Grinstein G (1992) *Phys Rev Lett* **69**: 3232; (1992) von Delft J, Henley CL, *ibid.*: 3236; Leuenberger MN, Loss D (2001) *Phys Rev B* **63**: 054414
- [16] Barbara B, Chudnovsky EM (1990) *Phys Lett A* **145**: 205

- [17] Krive IV, Zaslavskii OB (1990) J Phys Condens Matter **2**: 9457
- [18] Awschalom DD, Smyth JF, Grinstein G, DiVincenzo DP, Loss D (1992) Phys Rev Lett **68**: 3092; (1993) *ibid.* **71**: 4279(E)
- [19] Gider S, Awschalom DD, Douglas T, Mann S (1995) Science **268**: 77
- [20] Chiolero A, Loss D (1998) Phys Rev Lett **80**: 169
- [21] Meier F, Loss D (2001) Phys Rev Lett **86**: 5373
- [22] Meier F, Loss D (2001) Phys Rev B **64**: 224411
- [23] Honecker A, Meier F, Loss D, Normand B (2001) preprint cond-mat/0109201 (to be published in Eur Jour Phys B)
- [24] Grover LK (1997) Phys Rev Lett **79**: 325; *ibid.*: 4709; (1998) Phys Rev Lett **80**: 4329
- [25] Paulsen C, Park JG (1995) in *Quantum Tunneling of Magnetization*, edited by L. Gunther and B. Barbara (Kluwer, Dordrecht): p. 189
- [26] Paulsen C, Park JG, Barbara B, Sessoli R, Caneschi A (1995) J Magn Magn Mater **140-144**: 379
- [27] Novak MA, Sessoli R (1995) in *Quantum Tunneling of Magnetization*, edited by L. Gunther and B. Barbara (Kluwer, Dordrecht): p. 171
- [28] Sessoli R, Gatteschi D, Caneschi A, Novak MA (1993) Nature (London) **365**: 141
- [29] Novak MA, Sessoli R, Caneschi A, Gatteschi D (1995) J Magn Magn Mater **146**: 211
- [30] Hernández JM, Zhang XX, Luis F, Bartolomé J, Tejada J, Friedman JR, Sarachik MP, Ziolo R (1996) Europhys Lett **35**: 301
- [31] Barbara B, Wernsdorfer W, Sampaio LC, Park JG, Paulsen C, Novak MA, Ferré R, Mailly D, Sessoli R, Caneschi A, Hasselbach K, Benoit A, Thomas L (1995) J Magn Magn Mater **140-144**: 1825

- [32] Villain J, Hartmann-Boutron F, Sessoli R, Rettori A (1994) Europhys Lett **27**: 159
- [33] Fort A, Rettori A, Villain J, Gatteschi D, Sessoli R (1998) Phys Rev Lett **80**: 612
- [34] Luis F, Bartolomé J, Fernández F (1998) Phys Rev B **57**: 505
- [35] Hartmann-Boutron F, Politi P, Villain J (1996) Int J Mod Phys B **10**: 2577
- [36] Garanin DA, Chudnovsky EM (1997) Phys Rev B **56**: 11102
- [37] Hernández JM, Zhang XX, Luis F, Tejada J, Ziolo R, Phys Rev B **55**, 5858 (1997).
- [38] Barra AL, Gatteschi D, Sessoli R (1997) Phys Rev B **56**: 8192
- [39] Zhong Y, Sarachik MP, Friedman JR, Robinson RA, Kelley TM, Nakotte H, Christian-son AC, Trouw F, Aubin SMJ, Hendrickson DN (1999) J Appl Phys **85**: 5636
- [40] Barra A-L, Debrunner P, Gatteschi D, Schulz CE, Sessoli R (1996) Europhys Lett **35**: 133
- [41] Sangregorio C, Ohm T, Paulsen C, Sessoli R, Gatteschi D (1997) Phys Rev Lett **78**: 4645
- [42] Ohm T, Sangregorio C, Paulsen C (1998) Europhys J **B6**: 595; (1998) J Low Temp Phys **113**: 1141
- [43] Landau LD (1932) Phys Z Sowjetunion **2**: 46; Zener C (1932) Proc R Soc London A **137**: 696
- [44] Shimshoni E, Gefen Y (1991) Annals of Physics **210**: 16
- [45] Averin D, Bardas A (1995) Phys Rev Lett. **75**: 1831
- [46] Crothers DS, Huges JG (1977) J Phys. **B10**: L557; Nikitin EE, Umanskii SYa (1984) *Theory of Slow Atomic Collisions* (Springer, Berlin)
- [47] Garg A, Onuchi NJ, Ambegaokar V (1985) J Chem Phys. **83**: 4491

- [48] Gefen Y, Ben Jacob E, Caldeira AO (1987) Phys Rev B **36**: 2770
- [49] Kayanuma Y (1987) Phys Rev Lett. **58**: 1934
- [50] Ao P, Rammer J (1989) Phys Rev Lett. **62**: 3004; (1991) Phys Rev B **43**: 5397
- [51] Shimshoni E, Stern A (1993) Phys Rev B **47**: 9523
- [52] Leggett AJ, Chakravarty S, Dorsey AT, Fisher MPA, Garg A, Zwerger W (1987) Rev Mod Phys. **59**: 1
- [53] Caciuffo R, Amoretti G, Murani A, Sessoli R, Caneschi A, Gatteschi D (1998) Phys Rev Lett **81**: 4744
- [54] Taft KL, Delfs CD, Papaefthymiou GC, Foner S, Gatteschi D, Lippard SJ (1994) J Am Chem Soc **116**: 823
- [55] Caneschi A, Cornia A, Fabretti AC, Foner S, Gatteschi D, Grandi R, Schenetti L (1996) Chem Eur J **2**: 1379
- [56] Waldmann O, Koch R, Schromm S, Schüle J, Müller P, Bernt I, Saalfrank RW, Hampel F (2001) Inorg Chem **40**: 2986
- [57] van Slageren J, Sessoli R, Gatteschi D, Smith AA, Helliwell M, Winpenny REP, Cornia A, Barra A-L, Jansen AGM, Rentschler E, Timco GA (2002) Chem Eur J **8**: 277
- [58] Affronte M, Lasjaunias JC, Cornia A, Caneschi A (1999) Phys Rev B **60**: 1161
- [59] Cornia A, Jansen AGM, Affronte M (1999) Phys Rev B **60**: 12177
- [60] Normand B, Wang X, Zotos X, Loss D (2001) Phys. Rev. B **63**: 184409
- [61] Pilawa B, Desquiotz R, Kelemen MT, Weickenmeier M, Geisselmann A (1998) J Magn Magn Mat **177-181**: 748
- [62] Waldmann O, Schüle J, Koch R, Müller P, Bernt I, Saalfrank RW, Andres HP, Güdel HU, Allenspach P (1999) Inorg Chem **38**: 5879

- [63] Garg A (1993) Europhys Lett **22**: 205
- [64] Julien M-H, Jang ZH, Lascialfari A, Borsa F, Horvatić M, Caneschi A, Gatteschi D (1999) Phys Rev Lett **83**: 227
- [65] Cornia A, Fort A, Pini MG, Rettori A (2000) Europhys Lett **50**: 88
- [66] Loss D (1998) in *Dynamical Properties of Unconventional Magnetic Systems*, edited by A. T. Skjeltrop and D. Sherrington (Kluwer, Dodrecht): p. 29
- [67] Braun H-B, Loss D (1994) J Appl Phys **76**: 6177
- [68] Braun H-B, Loss D (1995) Europhys Lett **31**: 555
- [69] Braun H-B, Loss D (1996) Phys Rev B **53**: 3237
- [70] Braun H-B, Loss D (1996) J Appl Phys **79**: 6107
- [71] Braun H-B, Kyriakidis J, Loss D (1997) Phys Rev B **56**: 8129
- [72] Kyriakidis J, Loss D (1998) Phys Rev B **58**: 5568
- [73] Shor P (1994) *Proceedings of the 35th Annual Symposium on the Foundations of Computer Science* (IEEE Press, Los Alamitos): p. 124
- [74] Ahn J, Weinacht TC, Bucksbaum PH (2000) Science **287**: 463
- [75] Thiaville A, Miltat J (1999) Science **284**: 1939
- [76] Leuenberger MN, Loss D, Poggio M, Awschalom DD (2002) cond-mat/0204355
- [77] Salis G, Fuchs DT, Kikkawa JM, Awschalom DD, Ohno Y, Ohno H (2001) Phys Rev Lett **86**: 2677; Salis G, Awschalom DD, Ohno Y, Ohno H (2001) Phys Rev B **64**: 195304

FIGURES

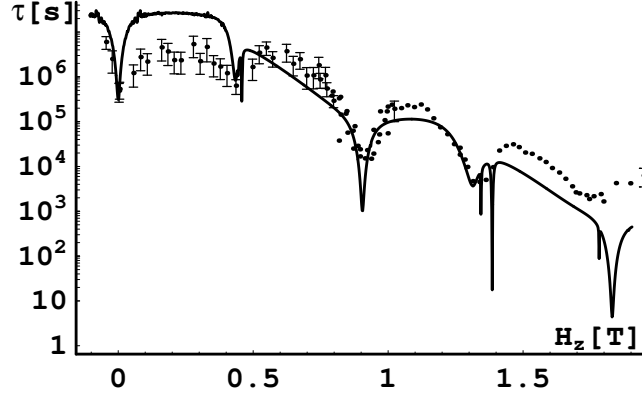


FIG. 1. Full line: semilogarithmic plot of calculated relaxation time τ as function of magnetic field H_z at $T = 1.9$ K. Dots and error bars: data taken from Ref. [8].

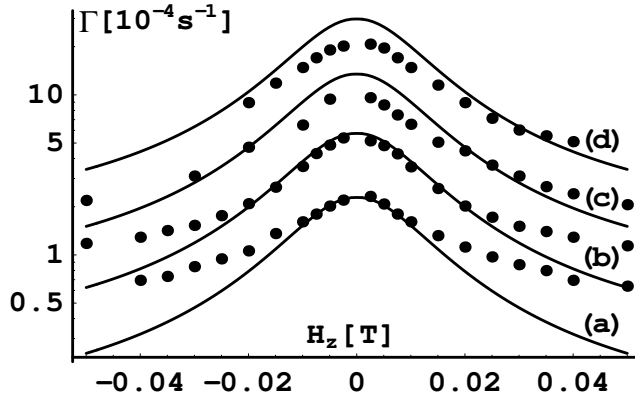


FIG. 2. Full lines: semilogarithmic plots of calculated relaxation rate $\Gamma = 1/\tau$ as function of H_z for the first resonance peak at (a) $T = 2.5$ K, (b) $T = 2.6$ K, (c) $T = 2.7$ K, and (d) $T = 2.8$ K. All peaks are of single Lorentzian shape. Dots: data taken from Ref. [7].

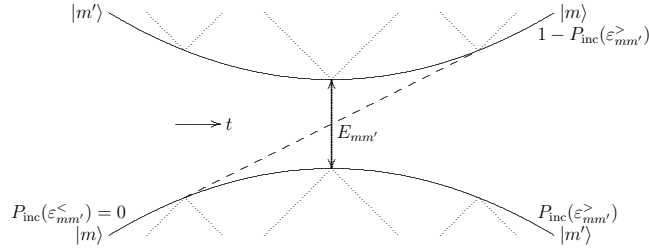


FIG. 3. Energy level crossing diagram for incoherent Zener transitions. Dotted lines: transitions due to interaction with environment, leading to a linewidth $\gamma_{mm'}$.

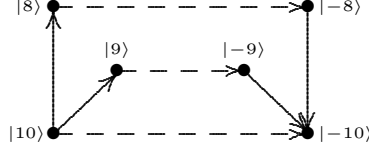


FIG. 4. Unbiased ($n = 0$) relaxation diagram for Fe_8 . Full (dashed) lines: thermal (tunneling) transitions.

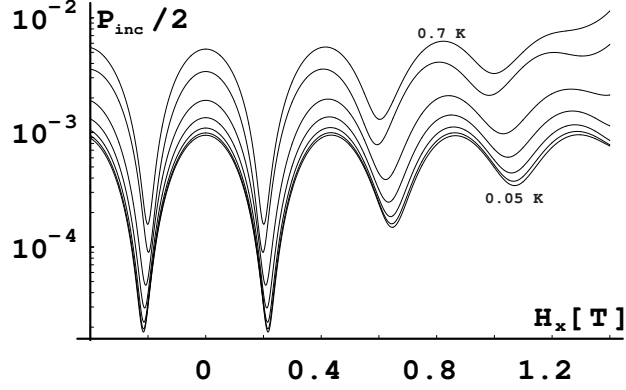


FIG. 5. Zener transition probability $P_{\text{inc}}(H_x)$ for temperatures $T = 0.7$ K, 0.65 K, 0.6 K, 0.55 K, 0.5 K, 0.45 K, and 0.05 K. The fit agrees well with data (Ref. [13]). Note that P_{inc} is equal to $2P$ in Ref. [13].

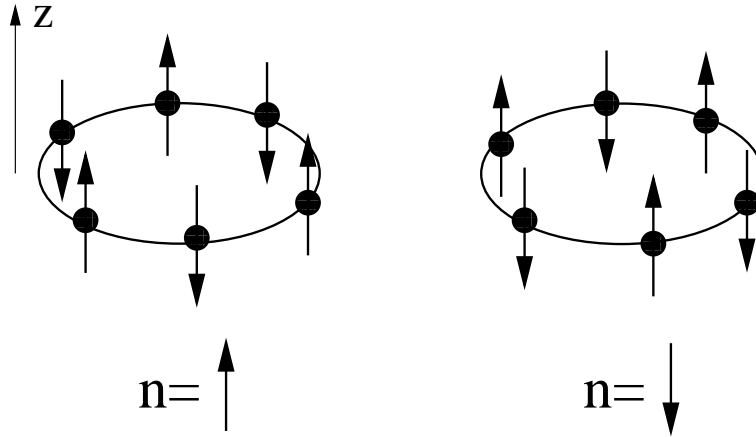


FIG. 6. The two degenerate classical ground state spin configurations of an antiferromagnetic molecular wheel with easy axis anisotropy.

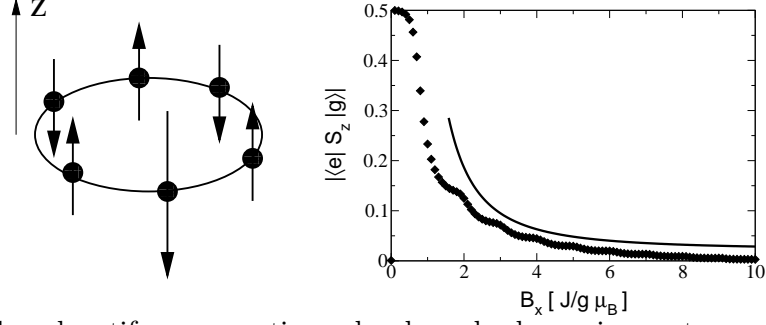


FIG. 7. The doped antiferromagnetic molecular wheel acquires a tracer spin which follows the Néel vector dynamics (left panel). Comparison of results obtained for the matrix element $|\langle e|\hat{S}_z|g\rangle|$ with a coherent state spin path integral formalism (solid line) and by numerical exact diagonalization (symbols) for $N = 4$, $s = 5/2$, $s' = 2$, $J' = J$, $k_z = k'_z = 0.055J$ (right panel).

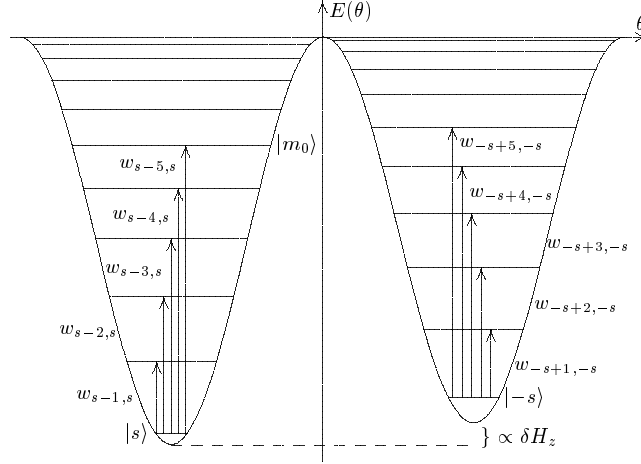


FIG. 8. Double well potential seen by the spin due to magnetic anisotropies in Mn_{12} . Arrows depict transitions between spin eigenstates driven by the external magnetic field \mathbf{H} .

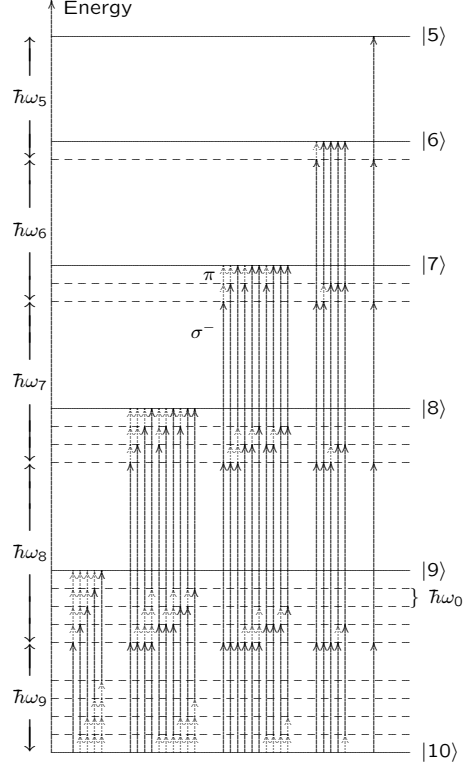


FIG. 9. Feynman diagrams \mathcal{F} that contribute to $S_{m,s}^{(5)}$ for $s = 10$ and $m_0 = 5$ describing transitions (of 5th order in V) in the left well of the spin system (see Fig. 8). The solid and dotted arrows indicate σ^- and π transitions governed by Eq. (20) and Eq. (19), respectively. We note that $S_{m,s}^{(j)} = 0$ for $j < n$, and $S_{m,s}^{(j)} \ll S_{m,s}^{(n)}$ for $j > n$.

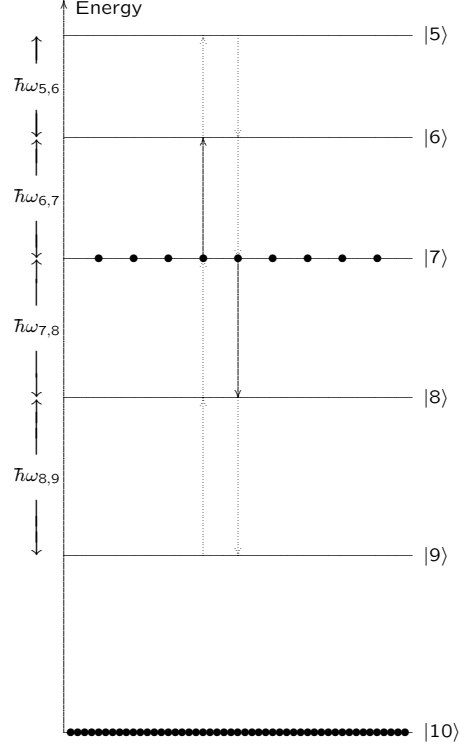


FIG. 10. Read-out of the information by ESR in the linear regime. In this example only the state $|7\rangle$ of the computational basis is populated. Thus only the transitions marked by solid arrows induce a response that can be observed in a ESR spectrum.